

# X-Ray Study of the Effect of Solute Atoms on Deformation Stacking Faults in Face-Centred Cubic Solid Solutions

著者	NAKAJIMA Koichi
journal or publication title	Science reports of the Research Institutes, Tohoku University. Ser. A, Physics, chemistry and metallurgy
volume	12
page range	309-323
year	1960
URL	<a href="http://hdl.handle.net/10097/26986">http://hdl.handle.net/10097/26986</a>

# X-Ray Study of the Effect of Solute Atoms on Deformation Stacking Faults in Face-Centred Cubic Solid Solutions\*

Kōichi NAKAJIMA

*The Research Institute for Iron, Steel and Other Metals*

(Received May 26, 1960)

## Synopsis

X-ray study of copper-nickel alloys pulverized by a ball mill and a stamp mill was carried out. Line peak shifts due to deformation stacking faults were observed by a Geiger counter spectrometer, and the stacking fault probability was calculated. The density of dislocation was estimated from the line broadening. From these experiments it was seen that the peak shift (or stacking fault probability) and the density of dislocation increased with the increase in solute content, reaching a maximum at 50~50 composition. The stacking fault energies of copper-nickel alloys were estimated from the equation proposed by Cottrell as a function of the solute content, which showed a downward concave curve; for example, the stacking fault energies of copper, copper 30 per cent-nickel and nickel were 30, 50 and 100 erg/cm<sup>2</sup> respectively.

In order to investigate on the segregation of solute atoms around the boundaries of stacking faults, small angle scattering experiments were carried out with copper-aluminium alloys severely cold-rolled at room temperature. And some observations on line profiles of the diffraction patterns were also made with powder samples of copper-aluminium, copper-nickel and copper-zinc alloys in order to see the effect of segregation of solute atoms on the diffractions. After all, it was concluded that in face-centred cubic solid solutions the solute atoms concentrated around faulted layers even at room temperature.

## I. Introduction

Owing to the improved experimental technique with the use of Geiger counter spectrometer, it is possible to perform some quantitative measurements on the change in X-ray diffraction pattern due to imperfect structure with sufficient accuracy, and accordingly, clearer information may be obtained on the defect of structure introduced by cold-working.

Recently, some theoretical and experimental studies of X-ray diffraction have been made on stacking fault introduced by the crystal growth,<sup>(1)</sup> the martensitic phase transformation,<sup>(2)</sup> and the plastic deformation<sup>(3)</sup> in crystals. Barrett<sup>(3)</sup> has shown that the stacking faults can be introduced in crystals during plastic deformation. Slip on (111) plane in face-centred cubic metals should introduce a deformation stacking faults in such a way that the sequence of (111) plane contains four hexagonal close-packed layers. Spreadbrough<sup>(4)</sup> has also proposed

\* The 984th report of the Research Institute for Iron, Steel and Other Metals.

(1) W. H. Zachariasen, *Acta Cryst.*, **1** (1948), 277.

(2) O. S. Edwards and H. Lipson, *Proc. Roy. Soc. (London)*, **180A** (1942), 268.

(3) C. S. Barrett, *Trans. Am. Inst. Mining Met. Engrs.*, **188** (1950), 123.

(4) J. Spreadbrough, *Phil Mag.*, **3** (1958), 1167.

a possible explanation of the occurrence of stacking faults in metals from the suggestion by Altmann et al.<sup>(5)</sup> that the metallic bond has greater directional characteristics, particularly when there are many bonding electrons available. Paterson<sup>(6)</sup> has calculated the effect of the stacking faults on X-ray diffraction, and observed a symmetric broadening and a small peak-shift due to the deformation stacking faults in (111) planes of face-centred cubic materials, but an asymmetrical line broadening and a negligibly small peak-shift in the case of twin stacking faults. Further, from their observations on cold-worked brass Warren and Warekois<sup>(7)</sup> have found some measurable peak-shift due to deformation stacking faults. Since then, X-ray diffraction studies on various face-centred cubic metals and alloys severely cold-worked have been made by Smallman and Westmacott<sup>(8)</sup>, Wagner<sup>(9)</sup>, and Christian and Spreadbrough<sup>(10)</sup>, and some informations on the faulting have been obtained by different methods of analysis. On the other hand, some experiments have been carried out by some workers on direct observations of the dislocations, the stacking faults, their arrangements and the motion of these defects. Whelan, Hirsch, Horne and Bollmann<sup>(11)</sup> observed the deformation stacking faults on slightly deformed thin sections of stainless steel directly by transmission electron microscope.

In a face-centred cubic lattice, an ordinary dislocation dissociates into a pair of half dislocation, leaving a stacking fault between them. Heidenreich and Schockley<sup>(12)</sup> emphasized that the crossing of the extended dislocation in different slip planes would be more difficult than that of unextended ones, by the aid of which slip hardening could be interpreted. The width of the separated half dislocations, which is determined by the balance of the repulsive force between them and the surface tension of the stacking fault, is different with different amounts of solute content and with different kinds of solute element. In general, the width is extended by the presence of solute atoms<sup>(8)</sup>.

Thus, the stacking faults may play an important role in work-hardening of metals and alloys, and it will be of great interest to investigate the solution hardening from the view point of the effect of solute atoms on the stacking fault. The present experiment was carried out with copper-nickel alloy to throw light upon these subjects.

- 
- (5) S. L. Altmann, C. A. Coulson and W. Hume-Rothery, *Proc. Roy. Soc.*, **240A** (1957), 145.
  - (6) M. S. Paterson, *J. App. Phys.*, **23** (1952), 805.
  - (7) B. E. Warren and E. P. Warekois, *Acta Met.*, **3** (1955), 473.
  - (8) R. E. Smallman and K. H. Westmacott, *Phil. Mag.*, **2** (1957), 669.
  - (9) C. N. J. Wagner, *Acta Met.*, **5** (1957), 427.
  - (10) J. W. Christian and J. Spreadbrough, *Proc. Roy. Soc.*, **240A** (1957), 1151.
  - (11) M. J. Whelan, P. B. Hirsch, R. W. Horne and W. Bollmann, *Proc. Roy. Soc.*, **240A** (1957), 524.
  - (12) R. D. Heidenreich and W. Schockley, *Report of a Conference of Strength of Solids* (1948), 57.

## II. Experimental procedure

Copper and nickel 99.9 and 99.8 per cent in purity respectively were used, and copper-nickel alloys of various compositions were pulverized at room temperature by a stamp and a ball mill. The material was first beaten by a stamp mill, and then the foils were pulverized by a ball mill made of selamix. To prevent the powdered sample from oxidation, the pulverization was carried out in benzene. The particle size and the homogeneity are important for the reproducibility of the experimental results of the X-ray diffraction, that is, fine particles with homogeneous size are absolutely necessary for the present experiments. The powder made by the above method was very fine and homogeneous in size, and the setting of the sample on a sample holder was easily carried out by compressing the sample without binder. The oxidation of the samples were preliminarily examined by X-ray photographs, and the results showed only diffraction lines from the specimen but none from oxides.

Measurements of X-ray diffraction were performed by XRD-5 diffractometer made by General Electric Co. in U.S.A. using Cu-K $\alpha$  radiation; the divergent and the receiving slit were respectively  $0.4^\circ \sim 3^\circ$  and  $0.02^\circ \sim 0.05^\circ$ , and the observation of the counts was made at every  $0.01^\circ$  by handling. Time required for 1,000 counts was adopted. Measurements of the shape and the peak-shift of (111) and (200) were made twice in every sample. The shift of (111) and (200) peaks due to cold-working was sharp enough to determine the centre of gravity to about  $0.01^\circ$ . The reproducibility of the results of the measurements was satisfactory.

According to Paterson theory<sup>(6)</sup>, random distribution in (111) planes of stacking faults due to plastic deformation of a face-centred cubic metal gives rise to symmetrical broadening and small peak-shift on diffraction of X-ray, from which a direct determination of stacking faults is possible. The relation between the peak-shift of any one diffraction line and the stacking fault probability can be obtained by the following equation after Warren and Warekois<sup>(7)</sup>:

$$\Delta(2\theta) = \pm \tan\theta \cos^2\phi (270\sqrt{3}/\pi^2)\alpha/h_3, \quad (1)$$

where  $\theta$  is the Bragg angle in degree,  $\phi$  the angle between the reflecting normal and the plane containing deformation stacking faults, and  $\alpha$  the stacking fault probability which is defined by the probability of finding a stacking fault between any two neighbouring layers,  $h_3 = |h+k+l|$ . Each powder pattern line is formed by the superposition of the diffraction with a given Bragg angle. For example, the {111} reflections consist of eight families, and the plane of  $|h+k+l| = 3N$  is not disturbed by the stacking fault and gives an ordinary crystalline reflection, whereas  $|h+k+l|^* = 3N \pm 1$  reflection gives a broadened reflection displaced towards

\* The effect of each component on the powder pattern can be determined directly from the value of  $|h+k+l|$  without explicit reference to the hexagonal indices, that is,  $|h+k+l| = 3N$ , and  $|h+k+l| = 3N \pm 1$  correspond to  $H_1 - H_2 = 3N'$ , and  $H_1 - H_2 = 3N' \pm 1$ , respectively.

higher or lower Bragg angle, where  $N$  is an integer. As the result, the  $\{111\}'$  reflections except (111) reflection are disturbed by stacking fault, that is,  $3/4$  of all  $\{111\}$  planes are effective, while all  $\{200\}$  reflections are affected by stacking faults. Thus, in  $\{111\}$  reflections the weighted mean,  $3/4 \times$  (the peak shift  $\{111\}'$  reflections due to the stacking faults), was used. Recently, Wagner<sup>(13)</sup> has proposed a similar equation on an assumption that the deformation and the twin stacking fault occur at random on any one set of  $\{111\}$  planes. For copper-nickel alloys examined with Cu-K $\alpha$  radiation, the relation between the peak-shift on  $\{111\}$  -  $\{200\}$  reflection due to deformation stacking faults and the stacking fault probability  $\alpha$  is approximately expressed as follows:

$$\Delta(2\theta_{200} - 2\theta_{111}) = -5\alpha \quad (2)$$

The appropriateness of the weighted mean of  $\{111\}$  reflections has been recognized on several assumptions, and a detailed discussion was recently made by Kakinoki<sup>(14)</sup>, as will be shown in a latter section.

It is generally recognized that the broadening of diffraction line for cold-worked metals is due mainly to lattice strains and fragmentation of grains. Warren and Averbach<sup>(15)</sup> first applied Fourier analysis of line shapes to the determinations of the strain, the particle size and the stacking fault in cold-worked metals. A similar analysis was carried out also by Williamson and Hall<sup>(16)</sup>; thus, methods have been developed for separating the effects of strain, particle size and stacking faults on the broadening, but these depend on the functional form assumed for the line broadening. Williamson and Smallmann<sup>(17)</sup> have investigated the effect of line shape and shown that in cold-worked metals the profile of the strain distribution lies between the extremes of the Cauchy and the Gaussian distribution, and considered the Cauchy type to be more probable. They discussed<sup>(16)</sup> this problem of line broadening by using Cauchy type distribution, and showed the following equation:

$$\begin{aligned} \beta &= \lambda/\epsilon \cos\theta + 2\xi \tan\theta, \\ \beta &= \beta_{\epsilon} + \beta_{\xi}, \end{aligned} \quad (3)$$

where  $\epsilon$  and  $\xi$  are respectively effective particle size and effective strain,  $\beta_{\epsilon}$  and  $\beta_{\xi}$  are the line width due to particle size broadening and strain broadening respectively, and  $\beta$  is the correct physical breadth, which is given experimentally by the Stokes method<sup>(18)</sup> for correcting instrumental broadening from an observed line broadening. In the plotting of  $\beta \cos\theta/\lambda$  against  $2\sin\theta/\lambda$ , the intercept gives the reciprocal of the effective particle size, while the slope gives the effective strain.

Several attempts have been made to determine the density of dislocation from

(13) C. N. J. Wagner, *Acta Met.*, **5** (1957), 477.

(14) J. Kakinoki, Unpublished. J. Kakinoki and Y. Komura, *J. Phys. Soc. Japan*, **9** (1954), 177.

(15) B. E. Warren and B. L. Averbach, *J. App. Phys.*, **21** (1950), 595.

(16) G. K. Williamson and W. H. Hall, *Acta Met.*, **1** (1953), 22.

(17) G. K. Williamson and R. E. Smallmann, *Acta Cryst.*, **7** (1954), 574.

(18) A. R. Stokes, *Proc. Phys. Soc.*, **61** (1948), 382.

the X-ray data. Williamson and Hall<sup>(19)</sup> have estimated the density of dislocation from the strain broadening, and obtained the following result:

$$\begin{aligned}\rho &= V/v_{real} = k\xi^2/Fb^2 \\ v_{real} &= v_e F,\end{aligned}\quad (4)$$

where  $V$  is the stored energy of the lattice due to cold-working, and  $v_e$  the energy of a free dislocation. Dislocations interact with one another so that their strain energies change, on an average, by a factor  $F$  depending on the arrangement of dislocations; in case a piled-up array  $F$  is equal to  $n$ , the number of dislocations in piled-up region, whereas in the case of uniform distribution of dislocations,  $F$  is equal to 1.  $b$  is Burgers vector,  $k$  a constant of order  $12A$ , and  $A$  a constant depending upon the shape of the strain distribution, and of the order of 2 for the Cauchy strain distribution, and of  $1/2\pi$  for the Gaussian distribution.

The stored energy  $V$  due to cold-working can also be deduced from the following equation:

$$V = 3E\bar{S}^2/2 = 3E(A\xi^2)/2, \quad (5)$$

where  $E$  is Young's modulus and  $\bar{S}^2$  the mean square strain in crystal.

### III. Results of experiments

Powdersample was annealed at various temperatures,  $100\sim 700^\circ\text{C}$  for 30 minutes in vacuum, and X-ray analysis was carried out at room temperature, and  $2\theta_{200} - 2\theta_{111}$  values of the samples changed as shown in Fig. 1. Fig. 2 shows the change

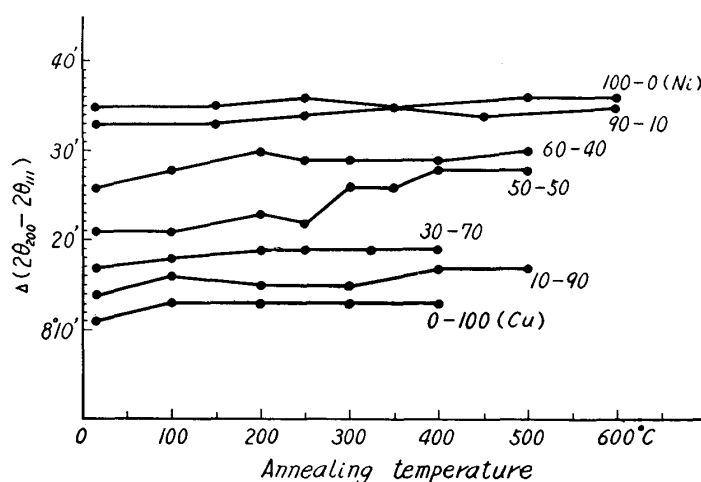


Fig. 1. Change in  $2\theta$  separation between (111) and (200) reflections of copper-nickel alloys. Points at the left refer to cold-worked states.

in the peak-shift due to cold-working as a function of solute content. From these results it will be seen that the peak-shift increases with the increase in solute content, reaching a maximum at about 50~50 composition. The stacking fault probability,  $\alpha$ , is obtainable from the peak-shift; it is, for example,  $10 \times 10^{-3}$  in

(19) G. K. Williamson and R. E. Smallmann, Proc. Roy. Soc., 183A (1955), 34.

50~50 alloy. This corresponds to an average of one stacking fault in every (111) plane containing one hundred atoms. Integral line breadth was obtained by graphical solution of the line shape in order to see the sum of the  $\alpha_1$  and the  $\alpha_2$  peak intensity.

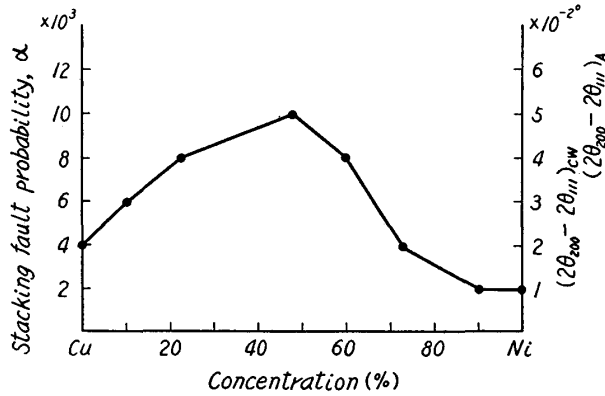


Fig. 2 Peak shifts between (111) and (200) reflections, and the stacking fault probabilities,  $\alpha$ , calculated from Eq. (2)  
 CW — Cold worked state  
 A — Annealed state

Fig. 3 shows the line broadening of spectra of copper-nickel alloys. The slope of these lines gives the effective strain in the matrix of the sample. Though the intercepts give the effective particle size  $\epsilon$  of respective samples, the change in the particle size with solute content is not given quantitatively by the analysis shown in Fig. 3. However, it will be seen qualitatively that the particle size decreases from about 1000 to 700Å in the [111] direction with increasing

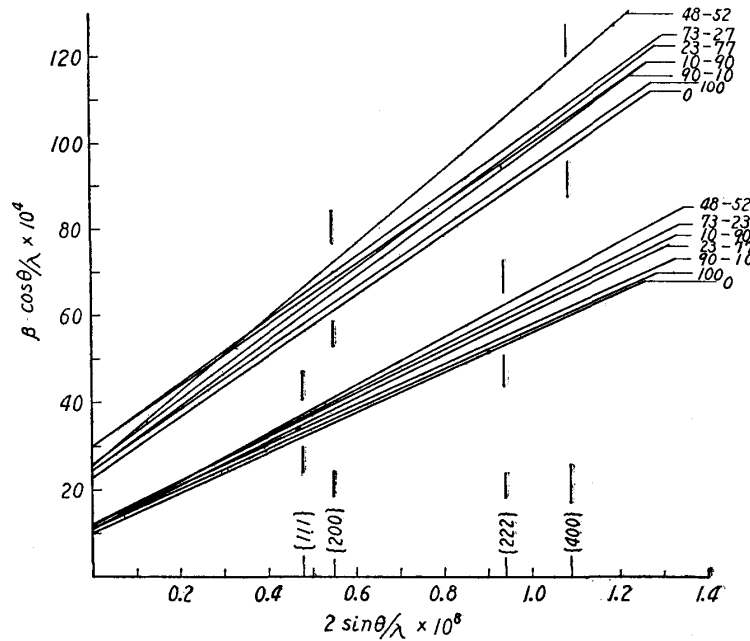


Fig. 3. Line broadening of the spectra of copper-nickel alloy.

solute content. An average particle size in the [111] direction of the alloy cold-worked at room temperature was of the order of 800Å. Fig. 4 shows the effective strain  $\xi$  as a function of the solute content, according to which the strain increases with increasing solute content, reaching a maximum at 50~50 composition.

The density of dislocation was calculated from Eq. (4) by using the effective strain obtained as above. In the case of a very fine powder sample, it will be natural that the dislocation is distributed uniformly. Therefore, in the present

case, the strain energy factor  $F$  can be taken as unity. The coefficient  $A$  was assumed to be 1, being a value between 2 in the Cauchy type distribution and  $1/2\pi$  in the Gaussian type distribution. The stored energy of the lattice due to cold-working and the density of dislocation calculated from Eqs. (4) and (5) are shown in Fig. 5, in which the elastic constants of copper-nickel alloys are those given by Shirakawa and Numakura.<sup>(20)</sup> It shows clearly that the density of dislocation and the stored energy increase with increasing solute content, reaching a maximum at about 50~50 composition.

When the density of dislocation and the stacking fault probability are known for a cold-worked sample, the equilibrium width of stacking fault will be obtained from the following relation of Cottrell<sup>(21)</sup>:

$$\tau = \mu a^2 / 24\pi\gamma, \quad (6)$$

where  $\mu$ ,  $a$  and  $\gamma$  are the shear modulus, the lattice parameter and the stacking fault energy respectively. On an assumption that the stacking fault probability corresponds to the fractional area of the hexagonal close-packed planes bounded by extended dislocation, the relation of dislocation density and the stacking fault probability is given by

$$\alpha = \rho d, \quad (7)$$

where  $d$  is the distance between the atoms of the nearest neighbour. From Eqs. (6) and (7) the following equation will be derived:

$$\alpha = \mu a^3 \rho / 24\sqrt{2} \pi \gamma, \quad (8)$$

that is, the stacking fault probability is a linear function of the density of dislocation, and therefore, the slope of the plot of the stacking fault probability against the density of dislocation should give the stacking fault energy, from

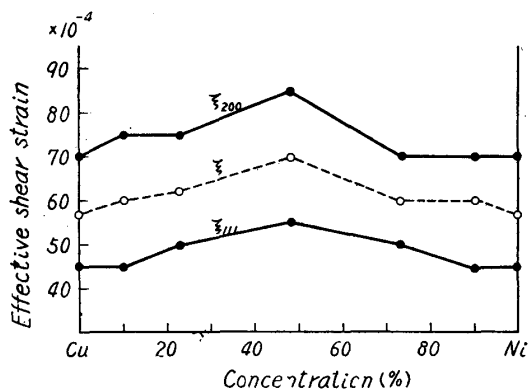


Fig. 4. Concentration change in effective strain  $\xi$ .

$\xi_{hkl}$ : Strain in the  $[hkl]$  direction.  
 $\xi$ : Average strain in the matrix defined by  $\frac{\xi_{200} + \xi_{111}}{2}$ .

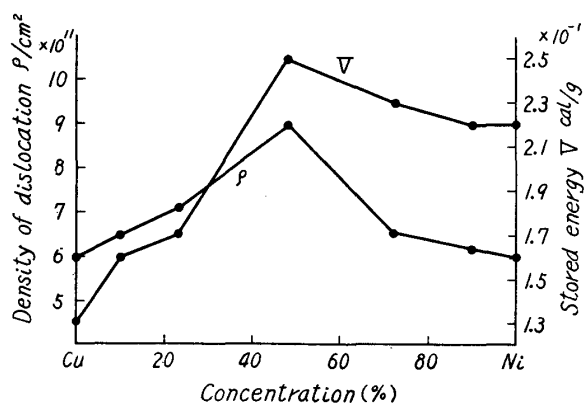


Fig. 5. Changes in density of the dislocation,  $\rho$ , and the stored energy,  $V$ , of copper-nickel alloys.

(20) Y. Shirakawa and K. Numakura, Sci. Rep. RITU, A9 (1957), 51.

(21) A. H. Cottrell, *Relation of Properties to Micro Structure*, (American Society for Metals, 1954), 131.



which the stacking fault energies in various compositions of copper-nickel alloys will be obtained. Fig. 6 shows the change in the stacking fault energy as a function of the solute content, from which it will be seen that the stacking fault energy has a decreasing tendency with a slight addition of copper in nickel,

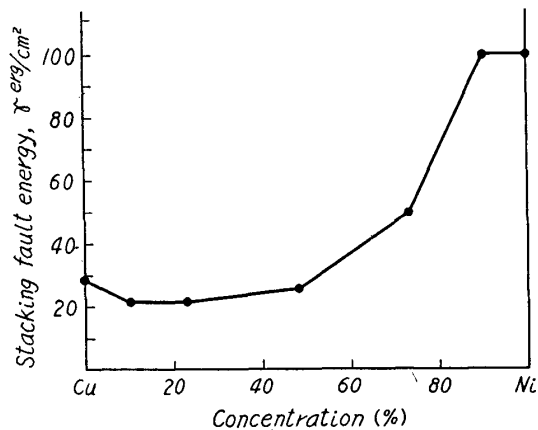


Fig. 6. Stacking fault energy.

energy has a decreasing tendency with a slight addition of copper in nickel, and that at higher solute content of about 50~50 composition, the stacking fault energy increases rapidly with increasing nickel content.

The peak-shift of the spectra of the sample due to cold-working was gradually released with the rise in annealing temperature, and in the case of a constant annealing temperature, the deviation of the peak position from the perfectly annealed state attains a certain constant value, which depends on the annealing temperature, as the time of annealing prolongs. Fig. 7 shows the change in the peak position of (111)

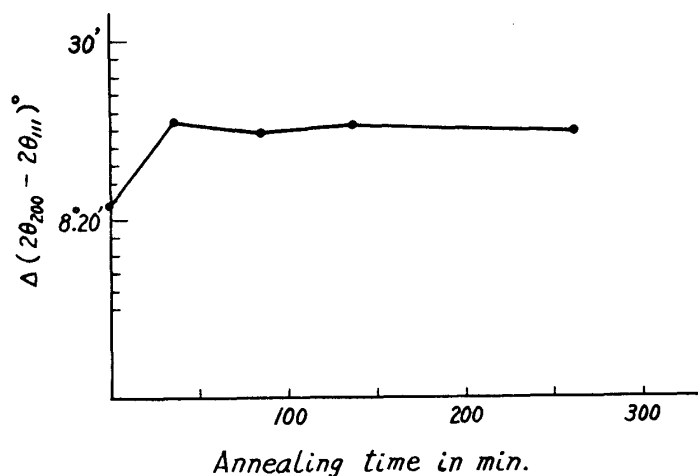


Fig. 7. Change in the  $2\theta$  separation between (111) and (200) reflections for copper-50 nickel alloys.

and (200) reflections of 50~50 alloy as a function of the time of annealing at 300°C. As shown in this figure, the peak-shift first increases rapidly and then becomes almost constant.

#### IV. Discussion

The adaptability of the weighted mean for obtaining the peak shift of {111} reflections mentioned above is based on the assumption that the peak intensities and the line shapes of all {111} reflections, which are affected by the stacking faults on (111) planes, are nearly equal to that of (111) reflection. However, Kakinoki<sup>(14)</sup> has pointed out that the intensity of (111) reflection relative to those of the other {111}' reflections depends markedly upon the stacking fault proba-

bility and on the number of atom layer of coherent range,  $N$ , showing the following relation for the relative intensity:

$$\begin{aligned} I^*(Nx) &= \frac{I(N, x \mp \delta)}{N^2} = \frac{1}{N^2} \{ND(x \mp \delta) + H(N, x \mp \delta)\} \\ &= \frac{1}{N^2} \frac{N(1-x^2) - 2x(1-x^N)}{(1-x)^2} \\ x &= (1-3\alpha+3\alpha^2)^{1/2}, \quad \tan\delta = (1-2\alpha)\sqrt{3} \end{aligned} \quad (9)$$

where  $D$  and  $H^{(14)}$  are the intensities of the diffuse scattering due to stacking fault and the higher order term respectively. According to this equation, with the increase in the number of atom layer of coherent range and in the stacking fault probability, the peak intensity of  $\{111\}$  reflection is contributed mainly by  $\{111\}$  reflection and is hardly affected by the other  $\{111\}'$  reflections. Therefore, when the number of layer  $N$  and the stacking fault probability  $\alpha$  are both small, the appropriateness of the weighted mean is not so poor, whereas with the increases of  $N$  and  $\alpha$ , it becomes poor, and in some cases, it will be necessary that  $\Delta 2\theta_{111} = 0$ . The stacking fault probability  $\alpha'$  obtained in this case and  $\alpha$  obtained by the equation of Warren and Warekois are connected by the following relation:

$$\alpha' = \left(1 + \frac{\tan\theta_{111}}{2\tan\theta_{200}}\right)\alpha \quad (10)$$

In the case of copper-nickel alloy,  $\alpha' = 1.4\alpha$ . This result shows that with the increases in the stacking fault probability  $\alpha$  and in the number of layer of coherent range  $N$ , the error in  $\alpha$  reaches about 40 per cent according to Eq. (2). It should be noticed that the appropriateness of the weighted mean is never good in the cases of large stacking fault probability and of large number of atom layer of coherent range.

The present experiments on copper-nickel alloys showed that the stacking fault probability  $\alpha$  reached a maximum value of 0.01 at 50~50 composition, and that the average particle size was of the order of 800Å. Consequently, the relative intensity is of the order of 0.4. This shows that the ratio of the peak intensity of  $\{111\}$  diffraction to those of other  $\{111\}'$  diffractions is about 4 to 10, and therefore, the use of Eq. (2) will not result in large error. For detailed analysis of this problem, it is necessary to have the intensity curve of each component on  $\{111\}$  diffractions.

As shown in Fig. 6, the stacking fault energy remains almost unchanged through the change in the content of the solute in copper rich side. However, the faulting energy increases rapidly with the increase in the solute content at about 70~30 composition. This seems qualitatively similar to the relation of magnetic transformation; in fact, the Curie point falls with increasing copper content and falls down to room temperature at 30 per cent copper in nickel. This problem will be of some interest in the effect of the stacking faults on the

mechanism of magnetization which is now under study.

The present experiments were carried out at room temperature. However, if the experiments are performed at lower temperatures, the line shift or the stacking fault probability will be altered; in fact, the stacking fault probability of cold-worked pure copper<sup>(7) (8)</sup> and nickel<sup>(22)</sup> in liquid nitrogen is about 2 times the value at room temperature. With increasing solute content in copper the peak-shift (or the stacking fault probability) and the density of dislocation increase gradually and reach a maximum at about 50~50 composition as shown in Figs. 2 and 5 respectively; in other words, these two quantities depend on the solute content. It may be considered that the solute atoms concentrate in the boundaries of faulted layer and anchor the stacking faults, and consequently, with increasing solute content the faults become difficult to disappear at room temperature. In fact, Suzuki<sup>(23)</sup> has pointed out that in a face-centred cubic solid solution the state of thermodynamical equilibrium in the faulted layer will be different from that in the matrix because of the concentration of solute atoms in the boundary of faulted layer. If this concept is valid, a small angle scattering due to the inhomogeneity of the structure will be observed. Arts and Jarvis<sup>(24)</sup> have verified Suzuki's effect from a measurement of electrical resistivity of deformed silver-gold alloy at low temperature. More direct verification of the solute concentration should be examined from a small angle scattering. However, copper and nickel have almost the same scattering factor, so the examination of the heterogeneous structure of the alloy by means of small angle scattering method is hardly possible. Copper-aluminium alloy was, therefore, used to examine the segregation of aluminium atoms around faulted layers at low temperatures. The specimens were severely cold-rolled at room temperature, the thickness being reduced to the order of  $30\mu$ , which is the optimum thickness of the material for X-ray experiment by  $\text{Cu-K}\alpha$  radiation. The first and the second slits were  $0.3 \times 2$  and  $0.15 \times 1 \text{ mm}^2$  respectively, and were separated from each other by 500 mm. The distance between the film and the specimen was also 500 mm. Photos. 1 and 2 show the X-ray photographs of the specimen after a certain heat treatment. Weak small angle scattering was actually observed in the specimens with aluminium of five per cent or more. Photo. 1 is the case of copper-8.5 per cent aluminium annealed at  $100^\circ\text{C}$  for 2 hours after severe cold-rolling, and Photo. 2 showing homogeneous Debye rings is an ordinary X-ray photograph obtained from the same sample as the above. The change in scattering intensity with the rise of annealing temperature was examined, and it was seen that in the case of copper-9 per cent aluminium the scattering was little observable when annealed at above  $200^\circ\text{C}$ , and that these phenomena corresponded to the recovery of asymmetrical line shape as will be mentioned later. However, it is doubtful whether the results obtained by the small angle scattering technique can directly be explained as the

(22) C. N. J. Wagner, *Rev. de Met.*, **55** (1958), 171.

(23) H. Suzuki, *Sci. Rep. RITU*, **A4** (1952), 455.

(24) W. H. Arts and R. K. Jarvis, *Acta Met.*, **2** (1954), 87.

segregation of the solute atoms around faulted layers, because the small angle scattering is caused not only by the heterogeneous structure in crystal but also by a wholly different process, namely, the double Bragg scattering. This scatter-

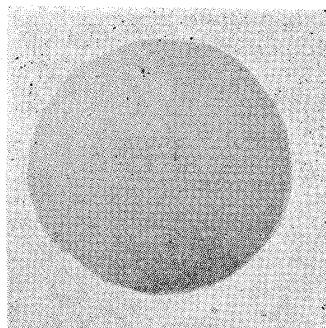


Photo. 1. X-ray photograph showing small angle scattering obtained from copper-8.5 per cent aluminium annealed at 100°C after severe cold-rolling. Thickness being about 50 $\mu$ .

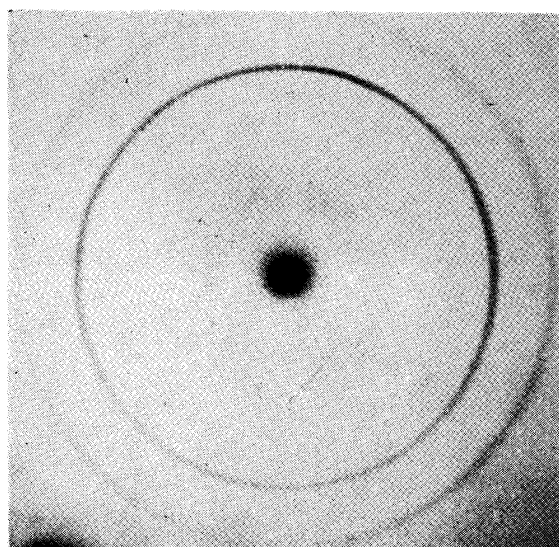


Photo. 2. X-ray photograph showing homogeneous Debye ring obtained from the same specimen as above.

ing takes place successively in the planes of the same family in two slightly dis-oriented blocks, or by two successive reflections from two different families of planes in different grains, and the double Bragg scattering<sup>(25)</sup> may not be neglected at all, compared with some weak true scattering due to heterogeneity in the sample. In fact, Atkinson<sup>(26)</sup> has clearly shown streaks in X-ray photographs obtained by a long-time exposure with heavily cold-rolled copper, and some of them did not pass through the trace of the direct beam. These streaks have completely been explained by the double Bragg reflection. Further, according

(25) Small angle scattering conference proceedings, *J. App. Phys.*, **30** (1959) For example, W. H. Robinson and R. Smoluchowski, p. 617; H. H. Atkinson, p. 637; A. Guier, p. 601.

(26) A. H. Atkinson, *Phil. Mag.*, **3** (1958), 476.

to his results, it is necessary to use the radiation of wave length greater than the maximum interplanar spacing of crystal, in order to measure the small angle scattering from an inhomogeneity of structure without the double Bragg scattering. Then, in the present case, the required wave-length must be larger than  $4.17\text{\AA}$ , and consequently, it is difficult to take only the true small angle scattering without the double Bragg scattering, provided that the radiation of wave-length of X-ray is used. However, if the double Bragg scattering is negligible compared with the true scattering, the above streaks will be absent. To clarify this circumstance some observations were made with the same sample under the experimental condition different from the preceding one: the first and the second slit were both of the size  $0.5 \times 3 \text{ mm}^2$  and the distance between them was 100 mm, and that between the film and the sample was 70 mm. Though the samples were exposed for about 100 hours, the streaks due to the double Bragg scattering were not observed. Accordingly, the observed small angle scattering might be the true scattering due to the segregation of the solute atom around faulted layers. Further, the small angle scattering due to defects of crystal lattice should be examined. The calculation of the small angle scattering from dislocations was carried out by some workers.<sup>(27)</sup> However, detailed experiment of small angle scattering from cold-worked metals by Atkinson<sup>(26)</sup> showed that most of the small angle scattering by X-ray were due to double Bragg scattering, and that the scattering from the defect of crystal lattice was not observable. Extending the Paterson theory to the case of segregation of solute atom around stacking faults,

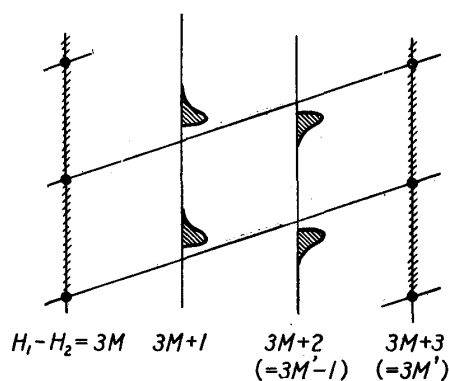


Fig. 8. Schematic diagram showing principal changes in reciprocal lattice induced by segregation. In the  $3M$  columns of reflexions a diffuse intensity band appears, while the reflexions in the  $3M \pm 1$  columns broaden asymmetrically.<sup>(29)</sup>

Willis<sup>(28)</sup> showed that the principal effect of the segregation was to make the reflexions asymmetrical, that is, the changes in the diffraction patterns caused by solute concentration in deformation faults give rise to weak diffuse streaks between reflections in the columns having  $H_1 - H_2 = 3M$ , and to asymmetry in the remaining reflections, as shown in Fig. 8; in the case of  $H_1 - H_2 = 3M$  the combined effects of faulting and segregation on the powder patterns make this component sharp and undisplaced, whereas in the case of  $H_1 - H_2 = 3M \pm 1$  it is broadened asymmetrically and displaced to higher or lower Bragg angles according to the sign. Therefore, the effect of the segregation

may be detected from the line profiles of powder diffraction lines. Figs. 9, 10

(27) For examples. H. H. Atkinson and P. B. Hirsch, *Phil. Mag.*, **3** (1958), 213, 862.

A. K. Seeger, *J. App. Phys.*, **30** (1959), 629.

(28) B. T. Willis, *Acta Cryst.*, **12** (1959), 683.

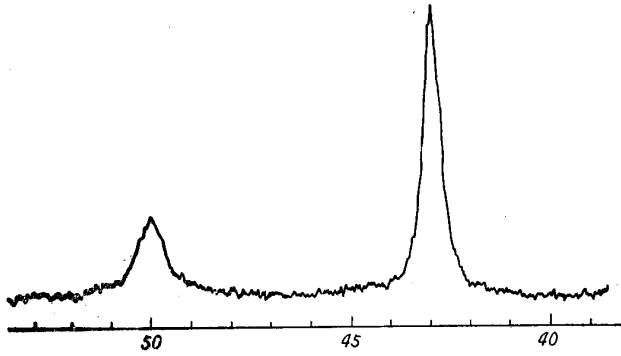


Fig. 9 (a) Line profile of  $\{111\}$  and  $\{200\}$  reflections in copper-2.5% aluminium without annealing treatment.

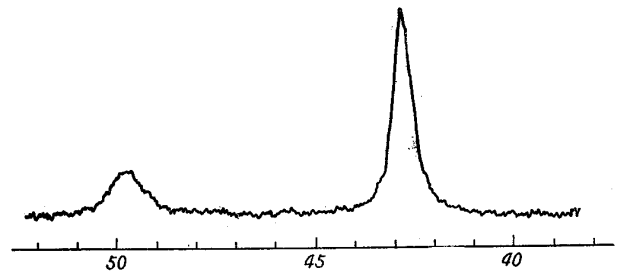


Fig. 9 (b) Line profile of  $\{111\}$  and  $\{200\}$  reflections in copper-5% aluminium without annealing treatment.

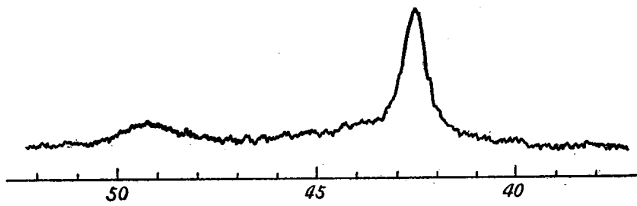


Fig. 10 (a) Line profile of  $\{111\}$  and  $\{200\}$  reflections showing asymmetrical reflection in copper-8.5% aluminium without annealing treatment.

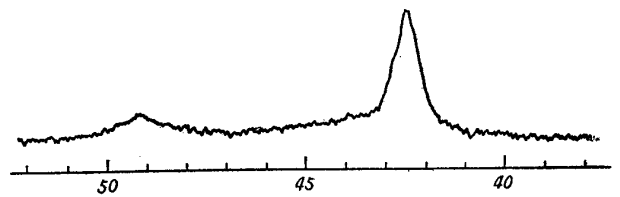


Fig. 10 (b) Line profile of  $\{111\}$  and  $\{200\}$  reflections showing asymmetrical reflection in copper-8.5% aluminium after annealing at 100°C for 2 hrs.

and 11 show the line profiles of  $\{111\}$  and  $\{200\}$  diffractions respectively of copper-aluminium, copper-nickel and copper-zinc alloys obtained by the Geiger counter spectrometer. Fig. 9(a) and 9(b) show the diffraction profiles obtained respectively with copper-2.5 per cent aluminium and copper-5 per cent aluminium alloys before and after heat treatment, from which it will be seen that the line broadening due to cold-working increases with increasing content of solute, but the asymmetry is hardly seen. However, in the case of the copper-8.5 per cent aluminium, the asymmetrical line broadening was observed as shown in Figs. 10 (a) and 10 (b) and the asymmetry disappeared through annealing at above 200°C, as shown in Figs. 10 (c) and 10

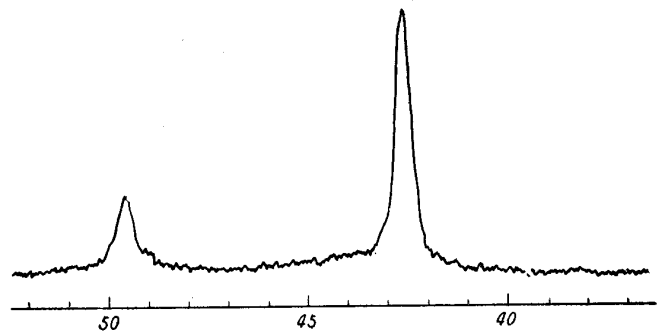


Fig. 10 (c) Line profile of  $\{111\}$  and  $\{200\}$  reflections on copper-8.5% aluminium after annealing at 200°C for 1 hr.

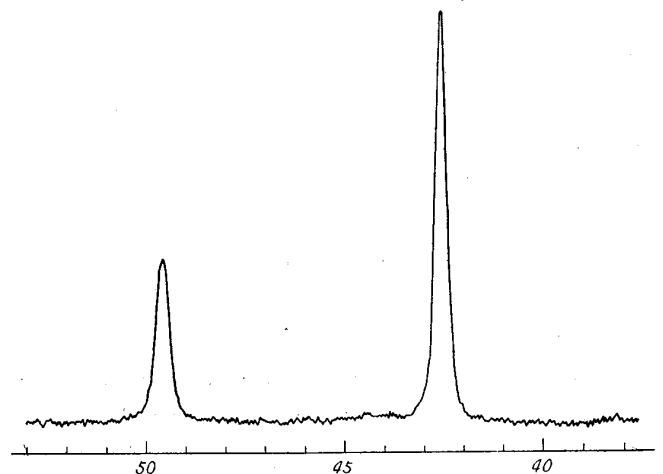


Fig. 10 (d) Line profile of  $\{111\}$  and  $\{200\}$  reflections on copper-8.5% aluminium after annealing at 500°C for 1 hr.

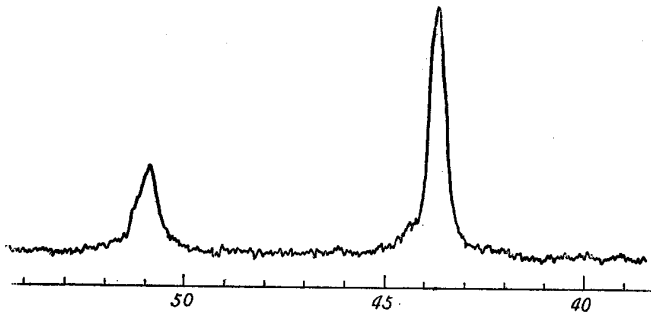


Fig. 11 (a) Line profile of  $\{111\}$  and  $\{200\}$  reflections in copper-48% nickel without annealing treatment.

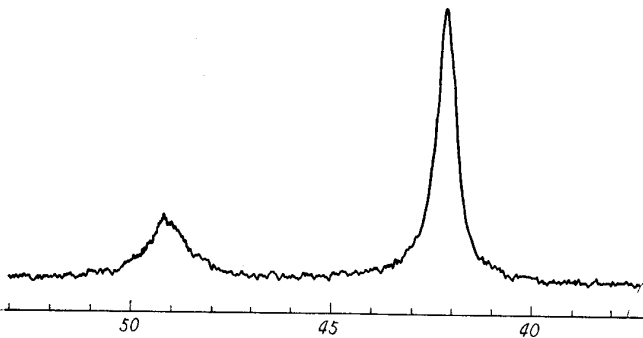


Fig. 11 (b) Line profile of  $\{111\}$  and  $\{200\}$  reflections in copper-37% zinc without annealing treatment.

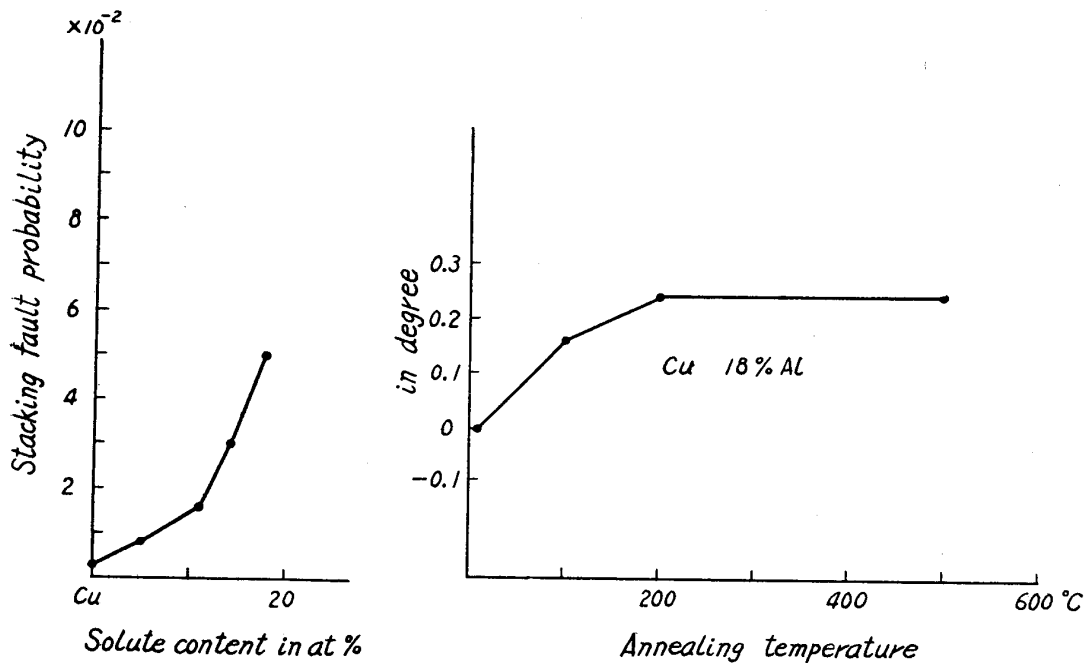


Fig. 12. Changes in stacking fault probability and  $2\theta$  separation on  $\{111\}$  and  $\{200\}$  diffraction. Values of  $2\theta$  separation at the left are for cold-worked material.

copper-nickel or copper-zinc alloy by means of X-ray experiments, whereas an experimental verification of the effect of segregation is possible, when copper-aluminium alloys are used. Thus, it is concluded that in face-centred cubic solid

(d). Fig. 12 shows the change in  $2\theta$  separation of  $\{111\}$  and  $\{200\}$  diffractions as a function of annealing temperature and the stacking fault probability of copper-aluminium alloys, from which it is seen that the peak-shift is released by the annealing at 200°C. A large asymmetrical broadening was not observed in the samples of copper-nickel and copper-zinc alloys, as shown in Figs. 11 (a) and 11 (b). The detection of the effect of segregation by X-ray measurement is difficult as mentioned above, when the scattering factors of the solvent and the solute atoms are nearly equal to each other, and therefore, the effect of the segregation cannot be observed with

solutions the solute atoms concentrate in the boundaries of faulted layers even at room temperature.

### Summary

- (1) X-ray study was carried out of copper-nickel and copper-aluminium alloys pulverized by a ball mill and a stamp mill.
- (2) Peak shifts of the diffractions of {111} and {200} were measured by Geiger counter.
- (3) The stacking fault probability increased with increasing solute content, reaching a maximum at about 50~50 composition.
- (4) Line broadening analysis was performed with the spectra of copper-nickel alloys, and the density of dislocation was calculated, which also increased with increasing solute content, reaching a maximum at about 50~50 composition.
- (5) The increase in the stacking fault probability with increasing solute content was interpreted to be due to the concentration of solute atom around faulted layer, which was verified by small angle scattering experiments with copper-aluminium alloys.
- (6) The effect of the segregation on the diffraction of the powder pattern with deformation faults suggested by Willis was examined.
- (7) In face-centred cubic solid solutions the solute atoms concentrate around the faulted layers even at room temperature.

### Acknowledgement

The author wishes to express his hearty thanks to Prof. S. Koda and Prof. Emeritus T. Sutoki for their kind guidance and suggestions, and also to Asst. Prof. Y. Shiota of the College of Arts and Science, Faculty of Education, Tohoku University for his zealous discussion throughout the course of this investigation, and to M. H. Hariu for his diligent aid throughout the course of the work. He acknowledges financial aids from the Ministry of Education.